Available online at www.sciencedirect.com
ScienceDirect
Polymer 49 (2008) 1910–1925
polymer
www.elsevier.com/locate/polymer

A physical insight into sonochemical emulsion polymerization with cavitation bubble dynamics

Narendra K. Morya [a], Parameswar K. Iyer [b], Vijayanand S. Moholkar [a,*]

[a] Department of Chemical Engineering, Indian Institute of Technology Guwahati, North Guwahati 781 039, Assam, India
[b] Department of Chemistry, Indian Institute of Technology Guwahati, Guwahati 781 039, Assam, India

Received 4 December 2007; received in revised form 17 February 2008; accepted 18 February 2008
Available online 21 February 2008

Abstract

This paper tries to explain the physical features of the sonochemical emulsion polymerization process by coupling experiments with different conditions (such as monomer type, saturation level of the medium and the type of bubbling gas) with a mathematical model for the radial motion of cavitation bubble. Experiments have been performed without any added chemical initiator or surfactant. Time variation of the mean size and size distribution of polymer particles in the emulsion have been used as a measure for the analysis. This measure is found to be governed by various parameters such as rate of radical production from the cavitation bubbles, magnitude of the microturbulence and shock waves produced by the cavitation bubbles, glass transition temperature of polymer and the population density of polymer particles. The relative magnitudes of these parameters vary significantly with the experimental conditions. This variation has been explained on the basis of results of simulation of radial motion of cavitation bubble. It is revealed that the mean particle size and size distribution of particles are manifestation of simultaneous and resultant influence of these parameters.

Keywords: Sonochemistry; Emulsion polymerization; Cavitation

1. Introduction

Sonochemical emulsion polymerization of various monomers (such as methyl methacrylate, butyl acrylate, vinyl acetate and styrene) has been extensively investigated in the past two decades (Kruus and Patraboy [1], Kruus et al. [2], Price et al. [3], Biggs and Grieser [4], Cooper et al. [5], Ooi and Biggs [6], Bradley and Grieser [7], Xia et al. [8], Price et al. [9], Zhang et al. [10], Zhang et al. [11], Yin et al. [12], Teo et al. [13]). Unlike conventional emulsion polymerization where the active free radicals are generated via a water-soluble chemical initiator, the sonochemical emulsion polymerization involves use of radicals formed out of transient collapse of cavitation bubbles to cause polymerization. Sonochemical initiation of polymerization reaction has been reported as early as 1950s by Lindstrom and Lamm [14], Henglein and Schulz [15] and Henglein [16]. Distinct merits of the sonochemical route for emulsion polymerization include faster polymerization at lower bulk liquid temperatures and elimination of the need of chemical initiator and costabilizer. Ultrasound manifests its effect on a liquid–liquid heterogeneous system (such as mixture of monomer and water in emulsion polymerization) in both physical and chemical ways through radial motion and transient collapse of cavitation bubbles (Suslick [17], Mason and Lorimer [18], Shah et al. [19]). The mechanical effect of ultrasound is the creation of intense microturbulence in liquid leading to the formation of fine emulsion of monomer in water, in the form of droplets typically in the range 50–500 nm. Under the influence of varying bulk liquid pressure with passage of ultrasound, the existing gas nuclei in the medium undergo intense volume oscillations. During the expansion phase, when the pressure at the gas–liquid interface falls below saturation vapor

* Corresponding author. Tel.: +91 361 2582258; fax: +91 361 2582291/2690762.
E-mail address: vmoholkar@iitg.ac.in (V.S. Moholkar).

0032-3861/$ - see front matter © 2008 Elsevier Ltd. All rights reserved.
doi:10.1016/j.polymer.2008.02.032

pressure, evaporation occurs and vapor of both water and dissolved monomer diffuses into the bubble. During the ensuing collapse phase, liquid vapor tends to condense at the bubble wall. However, during the final moments of transient bubble collapse, where the bubble wall velocity reaches closer to or even exceeds the velocity of sound in the liquid, the vapor at the center of the bubble has insufficient time to escape. This excess vapor is trapped or frozen in the bubble at the time of minimum radius reached during collapse, when the temperature and pressure inside the bubble are at the extreme ($\sim$5000 K and $\sim$500 bar). At these conditions, the vapor inside the bubble can decompose to yield radicals such as H, OH and HO_2 (Hart and Henglein [20,21], Suslick [22]). These radicals are released into the bulk medium with collapse of the cavitation bubble. The solutes (which, in the present situation, are the dissolved monomer molecules) in the boundary layer at the bubble–bulk interfacial region intercept these radicals. These solutes are basically the dissolved monomer and the surfactant (if added during polymerization). The addition of H and OH radicals to the monomer molecules results in the formation of monomeric radicals in the bulk medium. In the absence of a surfactant, these monomeric radicals can add to either another monomer molecule in the bulk or to a monomer droplet formed out of emulsification action of ultrasound and initiate polymerization. Finally, termination of the polymerization step occurs by reaction with another growing radical or by recombination. It needs to be mentioned that emulsification action of ultrasound obviates the need for surfactant in the bulk solution. Surfactant has basically two roles to play in the sonochemical polymerization system: first, it lowers the surface tension of the aqueous medium making dispersion of monomer into water easy, and secondly, surfactant molecules adsorb on the surface of the polymer nanoparticles. Repulsions between the adsorbed surfactant molecules avoid coalescence of polymer nanoparticles. Radial motion of cavitation bubbles driven by ultrasound creates intense microturbulence in the medium that helps formation of fine emulsion of two immiscible liquid phases, even in the absence of surfactant. Thus, need for surfactant – as far as first role is concerned – is obviated. Ultrasound, however, cannot be a surrogate for the second role.

The purpose of the present study is to provide a deeper insight into the mechanism of the sonochemical emulsion polymerization with simulation of the radial motion of a cavitation bubble. As can be understood from the discussion presented in previous paragraphs, the transient motion of the cavitation bubble is the basic underlying physical phenomenon in sonochemical emulsion polymerization. With experiments coupled to a mathematical model, which takes into account the essential physics and chemistry of the cavitation bubbles, we illuminate interesting physical aspects of the sonochemical emulsion polymerization process.

2. The overall physical picture and our approach

The present study addresses the physical features of sonochemical emulsion polymerization with a combined mathematical–experimental approach. The rate of formation of monomeric radicals via reaction $[OH^{\bullet}] + [M] \rightarrow [M]$ can be written as $-r_M = k_M[M][OH^{\bullet}]$. Rate of formation of monomeric radicals depends on the concentration of the monomer molecules and radicals (produced from cavitation bubble) at the bubble–bulk interfacial region. For sonochemical reactions, another factor comes into picture, which is the probability of interaction between the reactant (monomer in the present case) and the radicals. The radicals produced out of cavitation bubble are extremely reactive and react instantaneously after being released into the bulk medium with transient collapse of bubbles. However, in the present situation the bubble–bulk interface (which is hydrophobic in nature) is saturated with monomer molecules and the probability of interaction is quite high. With this, the controlling factor for the rate of formation of monomeric radical species is the rate of generation of radicals by the cavitation bubble. These radicals can induce polymerization reaction by adding to another monomer molecule (to give a growing radical) or to a droplet. The termination of the polymerization of the droplet may occur by reaction with another monomeric radical or growing radical. If the concentration of radicals is very high, the droplets are likely to be spot polymerized by set of radicals inducing and terminating polymerization reaction (Bradley and Grieser [7]).

The extent of formation of radical species out of cavitation bubble depends on two factors: (1) the extent of vapor (of both water and monomer) trapped in the bubble at the time of collapse and (2) the temperature peak attained during collapse, which decides the equilibrium composition of the various species resulting out of dissociation of vapor molecules entrapped in the bubble. In addition to the chemical effect, the radial motion of cavitation bubble also induces mechanical effects. These effects include: (1) creation of an intense oscillatory velocity field in the vicinity of the cavitation bubble and (2) generation of the shock wave, when the radial bubble motion comes to a sudden halt at the instance of minimum radius. Out of these, the first phenomenon is continuous one – occurring throughout the radial motion of bubble, while the second one is discrete – occurring only at the instances of minimum radius during radial motion. The oscillatory velocity field is responsible for shearing force, which disperses the monomer in the form of fine droplets. The shock waves, on the other hand, act towards disintegration of the polymer particles.

The approach in the present study is to assess the relative influence of the physical and chemical effects of the cavitation bubbles mentioned above on the outcome of the sonochemical emulsion polymerization process. The experimental technique that we adopt is as follows: (1) use of two monomers (viz. butyl acrylate and vinyl acetate) with widely varying water solubility and vapor pressure; (2) use of two kinds of gases for bubbling the reaction mixture: a monatomic gas (argon) and a diatomic gas (nitrogen); (3) variation in the dissolved gas concentration in the bulk liquid (water) medium. Simultaneously, we use a bubble dynamic model, which takes into account the heat and mass transfer effects during radial bubble motion to estimate the extent of radical production and

magnitude of the oscillatory velocity field and shock wave. The influence of these experimental techniques on the polymerization process has been estimated using particle size distribution as a measure – as it is the ultimate outcome or manifestation of the polymerization process. We have not dealt in this study with the kinetics of the polymerization (which would involve monitoring of the monomer conversion). Finally, we try to correlate the experimental and simulation results to get an insight into the physical features of the polymerization process.

3. Experimental section

3.1. Reagents

Two monomers viz. vinyl acetate (VA, Loba Chemie, >99%, synthesis grade) and butyl acrylate (BA, Loba Chemie, >99%, synthesis grade) were used. Prior to polymerization reaction, the inhibitor was removed by passing the monomer through a column of neutral alumina (Loba Chemie, mesh size 70–230). The monomer was transferred immediately to the reaction vessel after removal of the inhibitor. Two high purity (>99.9%) gases viz. argon and nitrogen were used for bubbling the emulsion during sonication. The monomer emulsions were prepared using Milli-Q water.

3.2. Experimental categories

For both VA and BA monomers, the polymerization experiments were divided into two categories: (1) using degassed (or unsaturated) aqueous medium and (2) using non-degassed (or saturated) aqueous medium. As stated earlier, two gases were used for bubbling the reaction mixture viz. (1) a monatomic gas (argon) and (2) a diatomic gas (nitrogen). By permutation – combination of these parameters, various sets of experiments are devised as follows:

(A) Butyl acrylate monomer
  (1) Unsaturated medium with nitrogen bubbling;
  (2) saturated medium with nitrogen bubbling;
  (3) unsaturated medium with argon bubbling;
  (4) saturated medium with argon bubbling.

(B) Vinyl acetate monomer
  (1) Unsaturated medium with nitrogen bubbling;
  (2) saturated medium with nitrogen bubbling;
  (3) unsaturated medium with argon bubbling;
  (4) saturated medium with argon bubbling.

3.3. Experimental system

The schematic of the experimental setup is shown in Fig. 1. A jacketed reactor made of borosilicate glass was used to conduct the polymerization reactions (dimensions: height – 120 mm; diameter – 50 mm; jacket thickness – 12 mm). A glass sparger was used to bubble the desired gas during sonication through water–monomer emulsion. This sparger used

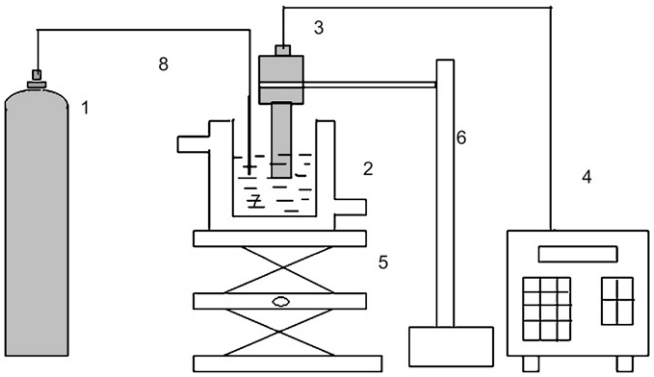

Fig. 1. Schematic representation of the experimental setup [Legends: 1. nitrogen cylinder; 2. jacketed reactor; 3. ultrasonic horn; 4. ultrasonic generator (processor); 5. laboratory jack; 6. laboratory stand; 7. reaction mixture; 8. gas passing to the aerator].

glass frit (pore size ~40 μm) to disperse the gas in the medium. The sonication of the monomer solution was done using a microprocessor-based and programmable ultrasonic processor (Sonics and Materials, Model VCX 500). This processor had a frequency of 20 kHz with the maximum power output of 500 W. The ultrasonic probe of the processor was fabricated from high grade titanium alloy and had a tip diameter of 13 mm. The processor had variable power output control, which was set at 20% during sonication resulting in net consumption of 100 W. It needs to be mentioned that this value corresponds to a theoretical maximum ultrasound intensity. The actual value of the ultrasound intensity in the medium was determined using calorimetry (Sivasankar et al. [23]). In addition, the processor had facility of automatic frequency tuning and amplitude compensation, which ensures constant power delivery to the ultrasound probe and the medium irrespective of the changes occurring in the medium. For a theoretical intensity of 100 W, the ultrasound probe produced an acoustic wave of 1.5 bar pressure amplitude.

3.4. Polymerization method

All polymerization reactions were carried out as batch reactions with a monomer concentration of 5% (w/w) in water without any added surfactant or chemical initiator. In a typical batch polymerization, an emulsion of 7.5 g of monomer and 142.5 g of Milli-Q water was prepared. For categories with saturated medium, the reaction mixture was bubbled with desired gas (argon or nitrogen) prior to sonication to remove the dissolved oxygen. During sonication, however, the bubbling flow rate was reduced to as low as 2 l/min using a rotameter. At this rate, the loss of volatile monomer such as VA from the solution due to diffusion with the bubbling gas is negligibly small. Another rationale behind low sparging rate of gas has been explained in Section 5. For categories of experiments with degassed medium, water was subjected to 700 mm Hg vacuum with intense stirring for 30 min prior to mixing of monomer. This procedure reduced the dissolved gas (basically air) content to very low value, with dissolved oxygen at <2 ppm. As in the case of experiments with saturated medium, desired gas was

bubbled through the water–monomer emulsion at a low rate of 2 l/min. The temperature of the medium at the beginning of sonication was 30 °C. The temperature rise during polymerization was restricted by circulating cooling water through the reactor jacket during sonication and using cycles of 5 min sonication followed by 5 min silent period. The temperature fluctuation during sonication was about ±5 °C. The total sonication time was only 20 min in order to avoid significant rise in dissolved gas content. Ten milliliters of samples were withdrawn from the reaction mixture at intervals of 5, 10 and 20 min of sonication. After addition of ~5 mg of inhibitor (hydroquinone) these samples were used for preparing the grids for SEM and TEM analyses. After placing a drop of sample over a grid, the grid was put in the flow of nitrogen at 30 °C for ~12 h. This caused evaporation of all water and unreacted monomer in the sample droplet leaving behind the polymer particles.

We would like to mention that in the absence of surfactant in reaction mixture, which also acts as a stabilizer preventing coalescence between the polymer particles (as noted earlier), some coalescence might occur. However, this effect is expected to be more or less the same for all samples, and thus, the trends observed in the particle size distribution remain unaffected.

3.5. Particle sizing

The average particle size in each sample along with the particle size distribution was determined from SEM and TEM images by sizing particles from each image and at least 10 images for each sample.

4. The mathematical model

Irradiation of liquid medium with ultrasound gives rise to phenomena of cavitation, which are growth, oscillation and transient collapse of tiny gas bubbles present in the medium. During the growth phase liquid vapor evaporates into the bubble. If the liquid contains a dissolved solute, it may also evaporate into the bubble. However, the extent of this evaporation will be determined by the partial pressure or equilibrium vapor pressure of solute at the bubble interface. In the ensuing compression phase, the vapor entered into the bubble condenses. This condensation is preceded by the diffusion of vapor molecules towards the bubble wall. At the final moments of collapse, the dynamics of bubble motion becomes extremely rapid and not all the vapors that have entered the bubble can escape. Thus, vapor entrapment occurs and the entrapped vapor is subjected to intense conditions of temperature and pressure generated inside the bubble. Under these conditions, the vapor molecules dissociate giving rise to various chemical species including free radicals (Hart and Henglein [20,21], Suslick [22]). These radicals can either diffuse out of the bubble or get mixed with the bulk liquid if the bubble fragments during transient collapse. Modeling of the generation of free radicals from cavitation bubbles has been an active area of research for past three decades and various authors have dealt with this matter with different approaches (Kamath et al. [24], Prasad Naidu et al. [25], Rajan et al. [26], Sochard et al. [27], Yasui [28,29], Gong and Hart [30], Moss et al. [31]). The most general treatment for the problem of vapor transport in large amplitude nonlinear motion of cavitation bubbles was presented by Storey and Szeri [32]. The principal result of analysis of Storey and Szeri was that vapor transport in the bubble is a diffusion-limited process. On the basis of this important result, Toegel et al. [33] developed a diffusion-limited model using boundary layer approximation, which forms the basis of the present study. This model has been validated against the full PDE simulations of Storey and Szeri [32].

We would like to mention that the overall polymerization effect is a manifestation of simultaneous oscillations of millions of bubbles present in the reaction medium. Such a system has extremely complicated physics with factors such as bubble–bubble coalescence, clustering, rectified diffusion affecting the overall effect. Another important parameter in this regard is the number density of bubbles. No experimental method has been developed yet, which can provide an estimate of this parameter, even with an order of magnitude accuracy. No model for the radial motion of a cavitation bubble has been developed so far, which takes into account all of these facets. Most of the bubble dynamic models are based on the radial motion of a single bubble. Although the single bubble analysis does not exactly reflect the entire physical phenomena in the system, it does provide a qualitative physical insight into the problem, as it addresses the essential physics of the problem such as heat transfer, mass transfer, vapor entrapment, etc.

Attempts of modeling physical or chemical effects of multi-bubble systems with single bubble models have been made by earlier authors. Ilyichev et al. [34] were the first to prove that all spectral characteristics of experimental acoustic cavitation (involving multi-bubble fields) can be explained with simulations of a single bubble. Later, Prasad Naidu et al. [25] and Rajan et al. [26] successfully explained the trends in the sonochemical oxidation of water–KI and water–KI–CCl_4 systems using single bubble model. More recently, Storey and Szeri [35] have also pointed out that experimentally observed trends in sonochemistry are reflected in the trends observed in the behavior of a single representative bubble. It must, however, be noted that single bubble models, due to simplifications involved in them, suffer from limitation that *no quantitative* predictions about reaction kinetics and yield can be made with them.

As far as objectives of the present study are concerned, single bubble approach for mathematical modeling is sufficient. A more rigorous approach relaxing assumptions and approximations made in this work would make quantitative changes to the analysis presented here. In the paragraphs below, we describe the model for simulation of radial motion of single cavitation bubble.

4.1. Radial motion of bubble

The radial motion of the bubble is described by the Keller–Miksis equation (Brennen [36], Prosperetti and Lezzi [37]).

$$\left(1-\frac{\mathrm{d}R/\mathrm{d}t}{c}\right)R\frac{\mathrm{d}^2R}{\mathrm{d}t^2}+\frac{3}{2}\left(1-\frac{\mathrm{d}R/\mathrm{d}t}{3c}\right)\left(\frac{\mathrm{d}R}{\mathrm{d}t}\right)^2 = \frac{1}{\rho_\mathrm{L}}\left(1+\frac{\mathrm{d}R/\mathrm{d}t}{c}\right)(P_\mathrm{i}-P_t)+\frac{R}{\rho_\mathrm{L}c}\frac{\mathrm{d}P_\mathrm{i}}{\mathrm{d}t}-4\nu\frac{\mathrm{d}R/\mathrm{d}t}{R}-\frac{2\sigma}{\rho_\mathrm{L}R} \quad (1)$$

R denotes the radius of the bubble at time t and ρ_L, σ, ν denote the physical properties of the liquid medium viz. the density, surface tension and kinematic viscosity, respectively. c is the speed of sound in the medium and the pressure inside the bubble (P_i) is written using van der Waal's type equation of state:

$$P_\mathrm{i}=\frac{N_\mathrm{tot}(t)\,kT}{\left[\frac{4\pi}{3}\left(R^3(t)-h^3\right)\right]} \quad (2)$$

k is the Boltzmann constant, N_tot denotes the total number of molecules in the bubble at time t and T is the temperature inside the bubble. h is van der Waal's hard core radius of various species in the bubble viz. nitrogen, oxygen, water and butyl acrylate or vinyl acetate. As an approximation we take a common value $h \approx R_0/8.86$ for all species, where R_0 is the equilibrium radius of bubble. A simple expression for P_t (the bulk pressure during ultrasound irradiation) is written as

$$P_t = P_0 - P_\mathrm{A}\sin(2\pi ft) \quad (3)$$

here P_0 is the ambient pressure and P_A and f denote the pressure amplitude and frequency of acoustic wave.

4.2. Mass transfer across bubble

During the radial motion of bubble, both gas and liquid (along with dissolved solute) vapor diffuse across the bubble wall. The transport of gas across bubble wall can be neglected for radial motions of duration of few acoustic cycles on the basis of difference in time scales, explained as follows: the time scale for the diffusion of gas is $\sim R_0^2/D$ where D is the diffusion coefficient. For representative values as $R_0 \sim 10$ μm, $D \sim 10^{-9}$ m^2/s, the time scale for the gas diffusion is 0.1 s, which is far higher than time scale of bubble dynamics ($\sim$50 μs for 20 kHz ultrasound wave). However, for radial motion of longer duration the transport of gas needs to be considered. Depending on the amplitude of the ultrasound wave driving the bubble motion and the extent of saturation of the liquid medium, the bubble may grow or shrink during oscillations due to transport of gas across the bubble. This process is called rectified diffusion, which has been investigated over past several decades for small amplitude oscillations of the bubble (Hsieh and Plesset [38], Eller and Flynn [39], Safar [40]). More recently, a generalized formulation of rectified diffusion is given by Lofstedt et al. [41] and Fyrillas and Szeri [42], which can be applied to large amplitude nonlinear motion of bubbles driven by the ultrasound waves of pressure amplitude greater than transient cavitation threshold (typically >1 bar for bubbles of size 5–20 μm). The major conclusions of Lofstedt et al. [41] and Fyrillas and Szeri [42] in the context of the present study are as follows: for acoustic pressure amplitudes >1 atm, the bubble grows during oscillations if the liquid medium is relatively saturated (≥80% or so). On the other hand, if the medium is unsaturated (relative saturation ≤30% or so) the bubble shrinks during radial motion. The parameters for the simulation of the radial bubble motion have been selected on the basis of these conclusions. For greater details on the mathematical analysis of rectified diffusion, we refer the reader to the original papers of Lofstedt et al. [41] and Fyrillas and Szeri [42]. Another important factor that affects the phenomenon of rectified diffusion is the surface tension of the liquid. Crum [43] reported that the presence of surfactant at the bubble–bulk interface enhances the growth rate of the bubble by rectified diffusion. Fyrillas and Szeri [42,44] proposed that the enhancement in growth rate is due to reduction in the interfacial resistance for mass transfer in the presence of surfactant. More recently, Lee et al. [45] have suggested that in addition to changes in surface tension and interfacial mass transfer in the presence of surfactant, effect of surface rheological properties may also contribute to enhancement in bubble growth rate.

In the present situation, both water and the dissolved monomer, either butyl acrylate or vinyl acetate, evaporate into the bubble. The surface temperature of bubble exceeds the bulk water temperature only for a very brief moment during collapse. On this basis, the present model divides the bubble into two parts: (1) a cold boundary layer in thermal equilibrium with liquid and (2) a hot homogeneous core. Due to their hydrophobic nature, the monomer molecules are driven towards the bubble–bulk interface, which also has a similar hydrophobic character (Bapat et al. [46]). Thus, the bubble–bulk interfacial region is always saturated with monomer molecules. The rate of change of water and monomer vapor molecules in the bubble is given by

$$\text{Water vapor}: \frac{\mathrm{d}N_\mathrm{w}}{\mathrm{d}t}=4\pi R^2 D_\mathrm{w}\left.\frac{\partial C_\mathrm{w}}{\partial r}\right|_{r=R} \approx 4\pi R^2 D_\mathrm{w}\left(\frac{C_\mathrm{wR}-C_\mathrm{w}}{l_\mathrm{diff}}\right) \quad (4)$$

$$\text{Monomer (either butyl acrylate or vinyl acetate) vapor}: \frac{\mathrm{d}N_\mathrm{M}}{\mathrm{d}t} = 4\pi R^2 D_\mathrm{M}\left.\frac{\partial C_\mathrm{M}}{\partial r}\right|_{r=R} \approx 4\pi R^2 D_\mathrm{M}\left(\frac{C_\mathrm{MR}-C_\mathrm{M}}{l_\mathrm{diff}}\right) \quad (5)$$

where l_diff is the instantaneous diffusive penetration depth and D_w and D_M are the effective diffusion coefficients for water vapor and monomer, respectively. Using dimensional analysis, the diffusive penetration depth is taken to be $l_\mathrm{diff} = \sqrt{D_\mathrm{w}t_\mathrm{osc}}$ for water molecules and $l_\mathrm{diff} = \sqrt{D_\mathrm{M}t_\mathrm{osc}}$ for monomer molecules. C_wR and C_MR is the equilibrium concentration of the water and monomer molecules at bubble wall, calculated assuming Raoult's law along with vapor pressures of individual (pure) components at bulk temperature. C_w and C_M are the concentrations of water and the monomer in the core of the bubble. The solubility of both butyl acrylate and vinyl acetate in water is rather small (0.002 g/ml for butyl acrylate and

0.023 g/ml for vinyl acetate). Since the solutions of monomer in water are rather dilute, we assume Raoult's law to hold good. Thus, the total vapor pressure of the monomer–water mixture is: $P_v = x_w P_w = x_M P_M$ (M – monomer, i.e. either BA or VA), where x_w and x_M are the mole fractions of water and monomer components in liquid, while P_w and P_M are the vapor pressures of water and monomer in pure form at the bulk temperature (T_o). We use following Antoine's equations for the calculation of P_w and P_M (in Pa) at temperature T (in K).

$$P_w = \frac{10^5}{760}\exp\left(18.3036 - \frac{3816.44}{T - 46.13}\right). \tag{6}$$

$$P_M\,(\text{Butyl acrylate}) = 10^5 \times 10^{(4.42683 - 1658.03/(T - 45.561))} \tag{7}$$

$$P_M\,(\text{Vinyl acetate}) = 10^5 \times 10^{(4.34032 - 1299.069/(T - 46.183))} \tag{8}$$

At the temperature of the experiment (30 °C), the vapor pressures of various components are as follows: water – 4222 Pa, vinyl acetate – 19 280 Pa, butyl acrylate – 978 Pa. The equilibrium concentrations of water and monomer molecules at bubble–bulk interface are written in terms of their partial pressures: $C_{wR} = (x_w P_w)/kT_0$ and $C_{MR} = (x_M P_M)/kT_0$.

Limits on diffusion length: At the instances of maximum and minimum radius, the bubble wall velocity is zero, and thus, an alternate expression is needed for diffusion length. We set this limit as R/π after identifying that vapor transport is governed by pure diffusion equation for condition $dR/dt = 0$. The limit R/π is set on the basis of solution of the diffusion equation in spherical geometry. For greater details on this, refer to the earlier papers (Kumar and Moholkar [47], Krishnan et al. [48]). Thus, the diffusion length for water molecules is: $\min(\sqrt{(RD_w)/(|dR/dt|)}, (R/\pi))$ while the diffusion length for the monomer molecules is: $\min(\sqrt{(RD_M)/(|dR/dt|)}, (R/\pi))$.

Determination of diffusion coefficient: In the present situation, we encounter a ternary system: either nitrogen–monomer–water or argon–monomer–water. The diffusion of nitrogen and argon across bubble wall is ignored for the reasons stated earlier. For water and monomer (either butyl acrylate or vinyl acetate), we first calculate the binary diffusion coefficients using kinetic theory of gases (Hirschfelder et al. [49]) with properties of boundary layer evaluated at bulk temperature (for greater details we refer the reader to earlier papers, i.e. Kumar and Moholkar [47], Krishnan et al. [48]). From these binary coefficients, the overall (or effective) diffusion coefficient for water (D_w) and the monomer (D_M) is calculated as

$$\frac{1}{D_w} = \frac{\varepsilon_{Gas}}{(1-\varepsilon_w)D_{w-gas}} + \frac{\varepsilon_M}{(1-\varepsilon_w)D_{w-M}} \tag{9}$$

$$\frac{1}{D_M} = \frac{\varepsilon_{Gas}}{(1-\varepsilon_M)D_{M-gas}} + \frac{\varepsilon_w}{(1-\varepsilon_M)D_{M-w}} \tag{10}$$

Here, ε denotes the mole fraction of the individual component. Subscripts M, gas and w represent monomer (either butyl acrylate or vinyl acetate), gas (either argon or N_2) and water, respectively. We provide in Table 1 some representative values of diffusion coefficients for water and monomer for given mole fractions of water, monomer and gas.

4.3. Heat transfer across bubble

The phenomena of heat transfer and mass transfer are analogous. Hence, the rate of heat transfer (Q) across bubble wall is

$$\frac{dQ}{dt} = 4\pi R^2 \lambda \left(\frac{T_0 - T}{l_{th}}\right) \tag{11}$$

where λ is the effective thermal conductivity of bubble contents and l_{th} is the thermal diffusion length: $\min(\sqrt{(R\kappa)/(|dR/dt|)}, (R/\pi))$. Thermal diffusivity ($\kappa$) is calculated as: $\kappa = \lambda/\rho_{mix}C_{p,mix}$, where ρ_{mix} and $C_{p,mix}$ represent the overall density and specific heat capacity of the mixture of various species in the bubble. The molecular specific heats C_p for various components are: $N_2 = 7k/2$, $Ar = 5k/2$ and $H_2O = 4k$. As the concentration of monomer dissolved in the solution is quite small, so will be the equilibrium pressure at the bubble–bulk interface and the diffusive flux of the monomer. The bubble contents will be dominated by either nitrogen or argon and water vapor. In view of this, we have not included the monomer as a component in the determination of the thermal conductivity and thermal diffusivity. The thermal conductivity of the bubble contents has been calculated considering only two components viz. nitrogen or argon and water vapor. To calculate the effective thermal conductivity, we first determine the thermal conductivity (λ) and viscosity (η_i) of the individual species using the kinetic theory of gases (again we refer readers to our earlier papers for greater details, e.g. Kumar and Moholkar [47] and Krishnan et al. [48]). The effective thermal conductivity of the mixture of species is given by the following relation (Wilke [50], Condon and Odishaw [51])

Table 1
Representative values for diffusion coefficient for water vapor and monomer at given mole fraction

Type of bubble	Mole fractions			Diffusion coefficients (m^2/s)
	Gas (N_2 or Ar)	Monomer (BA or VA)	Water vapor	
Nitrogen (10 μm)	$x_{N_2} = 0.9642$	$x_{VA} = 7.6842 \times 10^{-4}$	$x_W = 3.5 \times 10^{-2}$	$D_W = 2.1525 \times 10^{-5}$; $D_M = 1.0475 \times 10^{-5}$
	$x_{N_2} = 0.9648$	$x_{BA} = 2.2884 \times 10^{-6}$	$x_W = 3.5182 \times 10^{-2}$	$D_W = 2.1506 \times 10^{-5}$; $D_M = 1.7365 \times 10^{-5}$
Argon (10 μm)	$x_{Ar} = 0.9642$	$x_{VA} = 7.6842 \times 10^{-4}$	$x_W = 3.5 \times 10^{-2}$	$D_W = 2.0782 \times 10^{-5}$; $D_M = 8.5424 \times 10^{-6}$
	$x_{Ar} = 0.9648$	$x_{BA} = 2.2884 \times 10^{-6}$	$x_W = 3.5182 \times 10^{-2}$	$D_W = 2.0763 \times 10^{-5}$; $D_M = 1.4266 \times 10^{-5}$

$$\lambda_{\mathrm{mix}} = \sum \frac{\varepsilon_{\mathrm{i}}\lambda_{\mathrm{i}}}{\sum \varepsilon_{\mathrm{j}}\phi_{\mathrm{ij}}} \tag{12}$$

where i, j = Ar or N_2 and H_2O, and

$$\phi_{\mathrm{ij}} = \frac{1}{\sqrt{8}}\left(1+\frac{m_{\mathrm{i}}}{m_{\mathrm{j}}}\right)^{-1/2}\left[1+\left(\frac{\eta_{\mathrm{i}}}{\eta_{\mathrm{j}}}\right)^{-1/2}\left(\frac{m_{\mathrm{i}}}{m_{\mathrm{j}}}\right)^{1/4}\right]^2 \tag{13}$$

where m_{i} and m_{j} are the molecular masses of various species.

4.4. Overall energy balance

During the radial motion, the bubble is an open system through which the water and monomer molecules diffuse. However, due to very low equilibrium vapor pressure (as a result of low solubility of monomer in water), the diffusive flux of water molecules across the bubble wall is expected to be several magnitudes higher than that of monomer molecules. Thus, we write the energy balance for the bubble on the basis of binary system: Ar/N_2-H_2O, not incorporating the monomer molecules in the energy balance. The total energy balance for the bubble content is

$$\frac{\mathrm{d}E}{\mathrm{d}t} = \frac{\mathrm{d}Q}{\mathrm{d}t} - \frac{\mathrm{d}W}{\mathrm{d}t} + h_{\mathrm{W}}\frac{\mathrm{d}N_{\mathrm{W}}}{\mathrm{d}t} \tag{14}$$

The total energy E is a function of temperature and volume of the bubble and the number of molecules of various species in it. The rate of change of E for the nitrogen bubbles is

$$\frac{\mathrm{d}E}{\mathrm{d}t} = \left(\frac{\partial E}{\partial N_{\mathrm{W}}}\right)_{N_{\mathrm{N_2}},V,T}\left(\frac{\mathrm{d}N_{\mathrm{W}}}{\mathrm{d}t}\right) + \left(\frac{\partial E}{\partial N_{\mathrm{N_2}}}\right)_{N_{\mathrm{W}},V,T}\left(\frac{\mathrm{d}N_{\mathrm{N_2}}}{\mathrm{d}t}\right) + \left(\frac{\partial E}{\partial T}\right)_{N_{\mathrm{W}},N_{\mathrm{N_2}},V}\left(\frac{\mathrm{d}T}{\mathrm{d}t}\right) + \left(\frac{\partial E}{\partial V}\right)_{N_{\mathrm{W}},N_{\mathrm{N_2}},T}\left(\frac{\mathrm{d}V}{\mathrm{d}t}\right) \tag{15}$$

where V is the volume of the bubble and $N_{\mathrm{N_2}}$ and N_{W} are the number of nitrogen and water molecules in the bubble. In the case of argon bubble, a similar type of expression can be written with N_2 replaced by Ar. We ignore the transport of nitrogen molecules across bubble for the reasons stated earlier, and hence: $\mathrm{d}N_{\mathrm{N_2}}/\mathrm{d}t = 0$. Moreover we identify thermodynamic relations

$$\left(\frac{\partial E}{\partial T}\right)_{N_{\mathrm{w}},N_{\mathrm{N_2}},V} = C_{\mathrm{V,mix}} \text{ and } \left(\frac{\partial E}{\partial V}\right)_{N_{\mathrm{w}},N_{\mathrm{N_2}},T} = 0 \tag{16}$$

as the internal energy of an ideal gas is a principal function of composition and temperature. $(\partial E/\partial N_w)$ is the specific internal energy of water molecule (U_{w}) and is written as

$$\left(\frac{\partial E}{\partial N_{\mathrm{w}}}\right) = U_{\mathrm{w}} = N_{\mathrm{w}}kT\left(3+\sum_{i=1}^{3}\frac{\theta_i/T}{\exp(\theta_i/T)-1}\right) \tag{17}$$

with characteristic vibrational temperatures (θ_i) for water molecule are listed below. The enthalpy of the water molecule entering the bubble from cold interface is $h_{\mathrm{w}} = 4kT_{\mathrm{o}}$ and the rate of work done by the bubble ($\mathrm{d}W/\mathrm{d}t$) reduces to expansion work: $P_{\mathrm{i}}\mathrm{d}V$. Equating the RHS of Eqs. (14) and (15) above we get

$$C_{\mathrm{V,mix}}\frac{\mathrm{d}E}{\mathrm{d}t} = \frac{\mathrm{d}Q}{\mathrm{d}t} - P_{\mathrm{i}}\mathrm{d}V + (h_{\mathrm{w}} - U_{\mathrm{w}})\frac{\mathrm{d}N_{\mathrm{w}}}{\mathrm{d}t} \tag{18}$$

The specific heat of mixture $C_{\mathrm{V,mix}}$ is written in terms of the molecular specific heat of individual components (C_{Vi}) and the number of molecules of individual components (N_{i}) as: $C_{\mathrm{V,mix}} = \sum C_{\mathrm{V,i}}N_{\mathrm{i}}$ $\mathrm{i} = \mathrm{Ar}/\mathrm{N_2}, \mathrm{H_2O}$. The molecular specific heats C_{V} for various components in terms of characteristic vibrational temperatures (θ) are as follows:

$$C_{\mathrm{V,N_2}} = k\left[\frac{5}{2}+\frac{(\theta_{\mathrm{N_2}}/T)^2\exp(\theta_{\mathrm{N_2}}/T)}{(\exp(\theta_{\mathrm{N_2}}/T)-1)^2}\right]; \quad \theta_{\mathrm{N_2}} = 3350\ \mathrm{K} \tag{19}$$

$$C_{\mathrm{V,O_2}} = k\left[\frac{5}{2}+\frac{(\theta_{\mathrm{O_2}}/T)^2\exp(\theta_{\mathrm{O_2}}/T)}{(\exp(\theta_{\mathrm{O_2}}/T)-1)^2}\right]; \theta_{\mathrm{O_2}} = 2273\ \mathrm{K} \tag{20}$$

$$C_{\mathrm{V,W}} = k\left[3+\sum_{i=1}^{3}\frac{(\theta_i/T)^2\exp(\theta_i/T)}{(\exp(\theta_i/T)-1)^2}\right], \quad \theta_{1,\mathrm{W}} = 2295\ \mathrm{K}, \quad \theta_{2,\mathrm{W}} = 5255\ \mathrm{K} \text{ and } \theta_{3,\mathrm{W}} = 5400\ \mathrm{K} \tag{21}$$

4.5. Quantification of physical effects (microturbulence and shock wave)

The physical effect of radial motion of cavitation bubbles includes creating an intense oscillatory velocity field or microturbulence in the vicinity of the bubble, and secondly, formation of a shock wave during instances of minimum radius during bubble motion. We now define the magnitudes of these quantities in terms of radius of the bubble (R), the bubble wall velocity ($\mathrm{d}R/\mathrm{d}t$) and bubble wall acceleration ($\mathrm{d}^2R/\mathrm{d}t^2$), which can be calculated with bubble dynamic model presented above. As mentioned earlier, the radial motion of the bubble gives rise to an oscillatory velocity field in the close vicinity of the bubble. The velocity in the bulk liquid at a distance r from the bubble center is (Leighton [52], Young [53])

$$u(r,t) = \frac{R^2}{r^2}\left(\frac{\mathrm{d}R}{\mathrm{d}t}\right) \tag{22}$$

The above expression has been obtained by using a mass balance of the liquid moving between the bubble wall and a (fictitious) shell of liquid surrounding the bubble. The amplitude of the shock wave radiated by the bubbles of nitrogen or argon at a distance $r \gg R$ (far field) is written as

$$P_{\mathrm{s}}(r,t) = \frac{\rho_{\mathrm{L}}\mathrm{d}^2V_{\mathrm{b}}}{4\pi r\mathrm{d}t^2} = \rho_{\mathrm{L}}\frac{R}{r}\left[2\left(\frac{\mathrm{d}R}{\mathrm{d}t}\right)^2 + R\frac{\mathrm{d}^2R}{\mathrm{d}t^2}\right] \tag{23}$$

where V_{b} is the volume of the bubble. A representative value of r is taken as 1 mm.

4.6. Model parameters and numerical solution

Eqs. (1), (4), (5), (11) and (18) give a comprehensive model of radial motion of bubble with accompanying heat and mass transfer. The numerical solution of this model can be obtained by solving the equation using Runge–Kutta 4th order–5th order method (Press et al. [54]). The collapse of the cavitation bubble depends on several factors such as surface instability, local flow conditions and bubble population in the vicinity of the cavitation bubble. As a conservative estimate the condition for the bubble collapse is taken to be the first compression after an initial expansion. We estimate various model parameters as follows:

Pressure amplitude: The pressure amplitude of the acoustic wave (P_A) generated by ultrasound probe was determined as 1.5 bar using calorimetric techniques (Sivasankar et al. [23]). However, in a non-degassed or saturated medium, the ultrasound wave undergoes attenuation during its passage through the medium due the gas bubbles suspended in the medium (Prosperetti and Commander [55]). Therefore, for the non-degassed medium the actual acoustic wave amplitude sensed by the bubble is taken to be 1.25 bar, assuming $\sim$15% attenuation. For degassed medium, the attenuation is very low and a value of $P_A = 1.5$ bar has been used for simulations.

Frequency: The frequency (f) of the wave is taken as 20 kHz same as the frequency of the ultrasound processor.

Equilibrium radius of the bubble: The equilibrium radius (R_0) of the bubble is difficult to estimate. The dissolved gas content of the medium influences the size of the bubble through phenomenon of rectified diffusion. In an unsaturated medium, slow dissolution of gas inside the bubble makes the equilibrium bubble size to reduce with time. Reverse happens in a saturated medium, where the dissolved gas in the bulk liquid slowly accumulates inside the bubble making the equilibrium size grow with time. Taking into consideration these features, a representative value of R_0 is taken to be 10 μm for the unsaturated medium and 20 μm for the saturated medium.

Temperature of the medium: The temperature of the bulk medium is taken to be 30 °C. The temperature of the bulk liquid varies only slightly during sonication, and hence, we have neglected the effect of temperature variation in our analysis.

Equilibrium composition of the bubble contents: The composition of the bubble at the time of collapse is calculated assuming that thermodynamic equilibrium is reached in the bubble. This assumption is based on the difference between the time scale of bubble dynamics and time scale of various radical reactions, which is at least two orders of magnitude as shown in our previous study (Krishnan et al. [48]). Due to extremely fast reaction kinetics, the bubble content always remains at thermodynamic equilibrium. The equilibrium mole fraction of various species in bubble at the conditions of temperature and pressure at the first compression of the bubble was calculated using software FACTSAGE, which uses the free energy minimization algorithm proposed by Eriksson [56]. We would like to specifically mention that the equilibrium composition of the bubble contents at transient collapse has been determined on the basis of water and monomer molecules trapped in the bubble at the moment of collapse. For the nitrogen bubble, some species with nitrogen as a constituent element (e.g. N_2O, HNO, HNO_2, NH_2, etc.) also form out of dissociation of the molecules trapped in the bubble. However, these species are found in traces (with mole fraction $<10^{-10}$). Hence, these species have been ignored in equilibrium calculations.

5. Results

Polymerization experiments were done in eight sets with permutation – combination of three experimental parameters viz. type of monomer, type of gas used for bubbling the reaction mixture and the saturation level of the medium. Before presentation of the experimental results, we would like to point out the difference between the usual experimental procedure and the procedure adopted in this study for certain sets of experiments. The current procedure has distinct implications on the cavitation phenomena in the medium, which influences the outcome of the polymerization reaction and helps reveal some interesting features of the process. In the usual procedure, argon or nitrogen is bubbled through the reaction mixture prior to polymerization so as to remove the dissolved oxygen. This procedure leaves the reaction mixture saturated with bubbling gas. During polymerization, the gas is passed over the reaction mixture. In the present study, the gas continuously bubbled through the reaction mixture. For the experimental sets with saturated medium, the desired gas was bubbled vigorously through the reaction mixture prior to sonication to remove the dissolved oxygen. However, the bubbling gas flow rate was reduced to 2 l/min during sonication. In contrast, for the experimental sets with unsaturated medium, dissolved oxygen in the medium (i.e. water) was removed using vacuum, which left the medium unsaturated. Thereafter, the gas flow rate used for bubbling reaction mixture was essentially the same as for the experimental sets with saturated medium. In this situation, the bubbling gas provides nuclei for cavitation in the medium. The dissolved gas content of the unsaturated medium rises with bubbling of nitrogen or argon. In order to restrict this rise, the sonication was carried out for short duration (20 min) for both monomers. This procedure essentially maintains the medium unsaturated during sonication. The unsaturation of the medium influences the radial motion of bubbles through phenomena of rectified diffusion as explained in the previous section.

5.1. Experimental results

The time evolution of the polymer particle size (as measured using TEM images of the samples) is shown in Figs. 2 and 3. Representative TEM images of PBA and PVA are shown in Fig. 4. Some peculiar features of the time evolution of particle sizes with different experimental conditions can be observed as follows:

Experiments with saturated medium: (1) The mean particle sizes vary little with time, i.e. during the progress of the polymerization reaction. On relative basis, greater variation in the mean particle size with time is seen for PBA than PVA. (2)

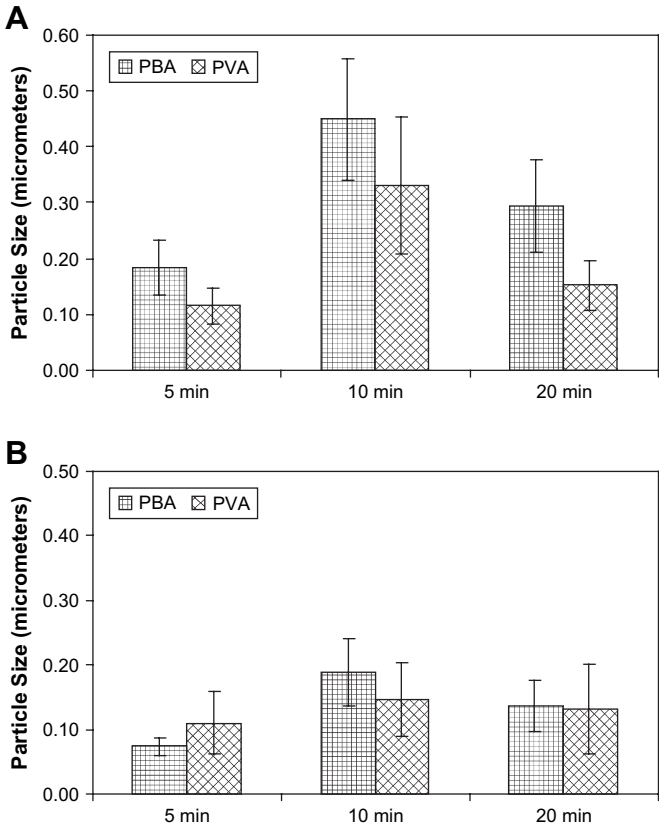

Fig. 2. Time evolution of PBA and PVA nanoparticles (A) in an unsaturated medium bubbled with nitrogen and (B) in a saturated medium bubbled with nitrogen.

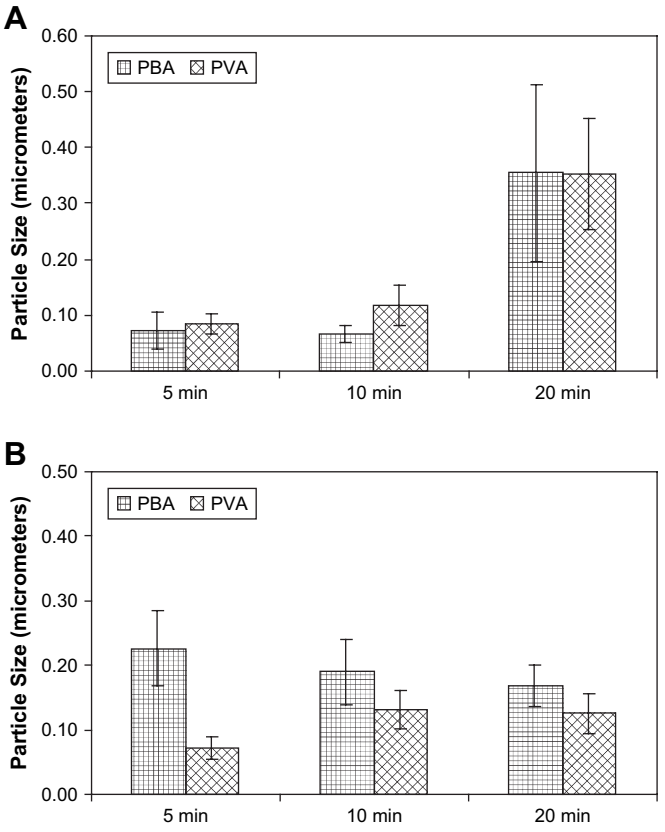

Fig. 3. Time evolution of PBA and PVA nanoparticles (A) in an unsaturated medium bubbled with argon and (B) in a saturated medium bubbled with argon.

The size distribution of the polymer particles at any instance (indicated by the error bars) is also small. (3) The mean particle size for PBA is slightly higher than for PVA. (4) The mean particle size for both PBA and PVA is higher for argon bubbling than that for nitrogen bubbling.

Experiments with unsaturated medium: (1) Large variation in the mean particle size is seen with time. Like saturated medium, greater variation in the mean particle size is seen for PBA than PVA. Moreover, fluctuation in particle sizes with time is more for argon bubbling than nitrogen bubbling. (2) The size distribution of the polymer particles at any particular time interval is also much wider than the saturated medium. (3) The mean particle size for both PBA and PVA after 20 min of sonication is found to be larger than the corresponding size in the saturated medium. (4) For 20 min of sonication, the mean size for PBA particles is higher than for PVA particles for nitrogen bubbling while for argon bubbling mean particle sizes for both PVA and PBA are similar.

5.2. Simulation results

Representative simulations of the radial motion of nitrogen bubble (size 20 μm with saturated medium) and argon bubble (size 10 μm with unsaturated medium) in the emulsions of BA and VA, respectively, are shown in Figs. 5 and 6. The summary of the simulation results is given in Tables 2 and 3 for the emulsions of BA and VA, respectively. These tables list the collapse conditions (i.e. the number of water and monomer molecules entrapped in the bubble and the temperature and pressure peak reached during collapse) along with the magnitude of the microturbulence velocity and the shock wave generated by the bubble. The equilibrium composition of various species at the conditions of transient collapse resulting out of dissociation of water and monomer molecules entrapped in the bubble is also shown in these tables. It is evident that several radical species capable of inducing polymerization are generated in the bubble. The total numbers of such species produced per single bubble can be calculated by the product of total molecules (monomer + water) entrapped and the equilibrium mole fraction. From the simulation results presented in Tables 2 and 3, we can identify some peculiar features and trends of the cavitation phenomena with varying dissolved gas content, the monomer type and the gas used for bubbling reaction mixture, as follows:

(1) The intensity of collapse of the smaller (10 μm) bubble representing unsaturated medium is much higher than that of larger (20 μm) bubble representing saturated medium. As a result, the rate of production of radicals in an unsaturated medium is higher than in the saturated medium. With larger rate of production of radicals, the polymerization kinetics is

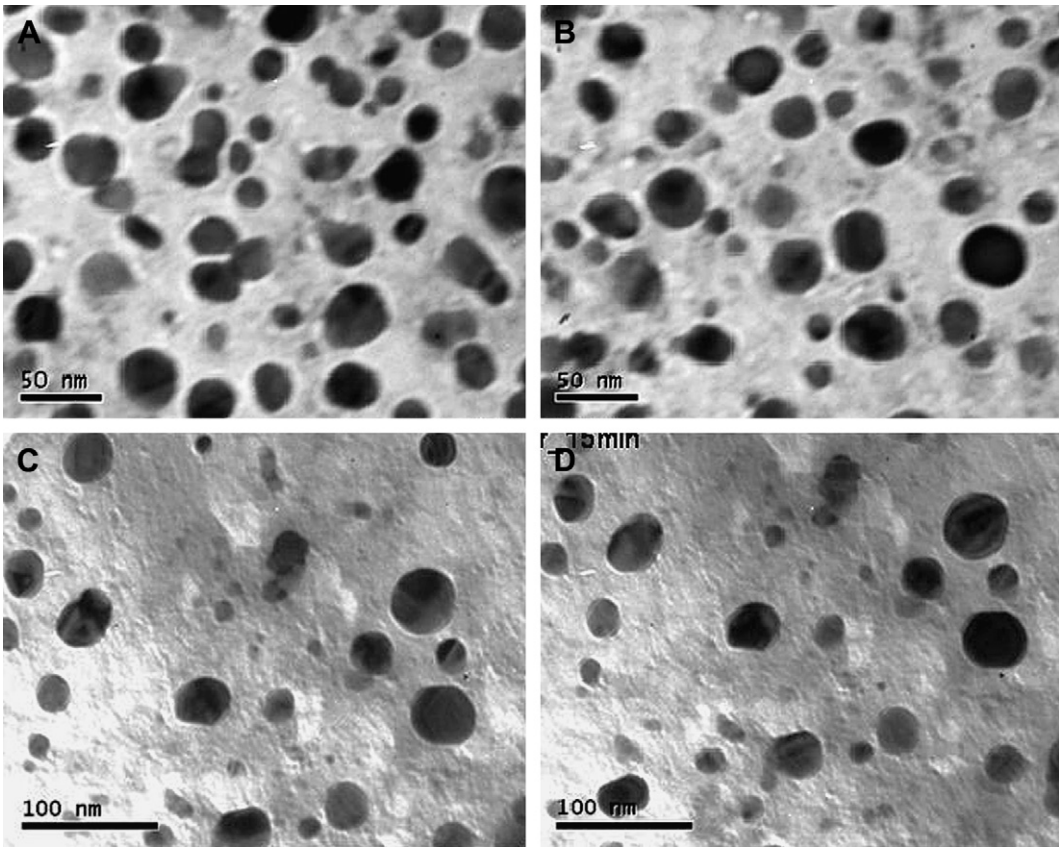

Fig. 4. Representative TEM micrographs for: (A) and (B) polybutyl acrylate (degassed medium with argon as bubbling gas) taken for 5 min sonication time and (C) and (D) polyvinyl acetate (degassed medium with argon as bubbling gas) taken for 15 min sonication time.

expected to be higher in an unsaturated medium. This is a combined effect of rectified diffusion and pressure amplitude of the ultrasound wave. In an unsaturated medium, the bubble continuously shrinks during oscillations due to transport of gas outside it. Moreover, the bubble population in an unsaturated medium is smaller resulting in lesser attenuation of the acoustic wave. Thus, the acoustic amplitude actually sensed by the bubble is higher, which contributes towards greater intensity of the collapse generating higher temperature peaks and greater equilibrium mole fraction of radicals. Moreover, a broad gamut of chemical species resulting out of dissociation of monomer and water molecules trapped in the bubble is seen.

On the other hand, for a 20 μm bubble the intensity of collapse is rather small giving relatively low temperature peaks. At these conditions, the bubble content mainly comprises of the species resulting out of dissociation of water molecules.

(2) For bubbles of any size (10 or 20 μm) the intensity of collapse of argon, which is a monatomic gas, is higher than that of nitrogen, which is a diatomic gas. Consequently, radical production rate in the bulk liquid medium with argon is higher than that of nitrogen. This is attributed to lower heat capacity of argon due to which it heats up to much greater extent than nitrogen.

(3) The velocity of microturbulence generated by the bubble is higher for 20 μm bubble than for 10 μm bubble. Thus, the shearing action of ultrasound is higher in a saturated medium. As a result, the monomer is distributed in the form of smaller droplets in a saturated medium. On the contrary, the droplet size of the monomer is expected to be larger in an unsaturated medium due to smaller microturbulence velocity.

(4) The magnitude of the shock waves, which act towards the disruption of the particles of size range in micrometers, is higher for argon bubbles than that for nitrogen bubbles. Moreover, the shock wave generated by a 10 μm bubble is larger than that by a 20 μm bubble. The enormity of the shock wave generated by the bubble is proportional to the intensity of collapse of the bubble. As noted earlier, this intensity is higher for a monatomic gas (argon) in an unsaturated medium.

(5) Evaporation of vinyl acetate molecules in the bubble is much higher than that of butyl acrylate. This result is attributed to both higher solubility and higher vapor pressure of vinyl acetate. Due to these features, the equilibrium vapor pressure (or partial pressure) of vinyl acetate at the gas–liquid interface is high; as a result of which the diffusive flux of vinyl acetate is large. Consequently, large numbers of vinyl acetate molecules get entrapped in the bubble during transient collapse and are subjected to the extreme conditions of temperature and pressure reached during collapse. At these conditions, the pyrolytic decomposition of vinyl acetate in the bubble results in much

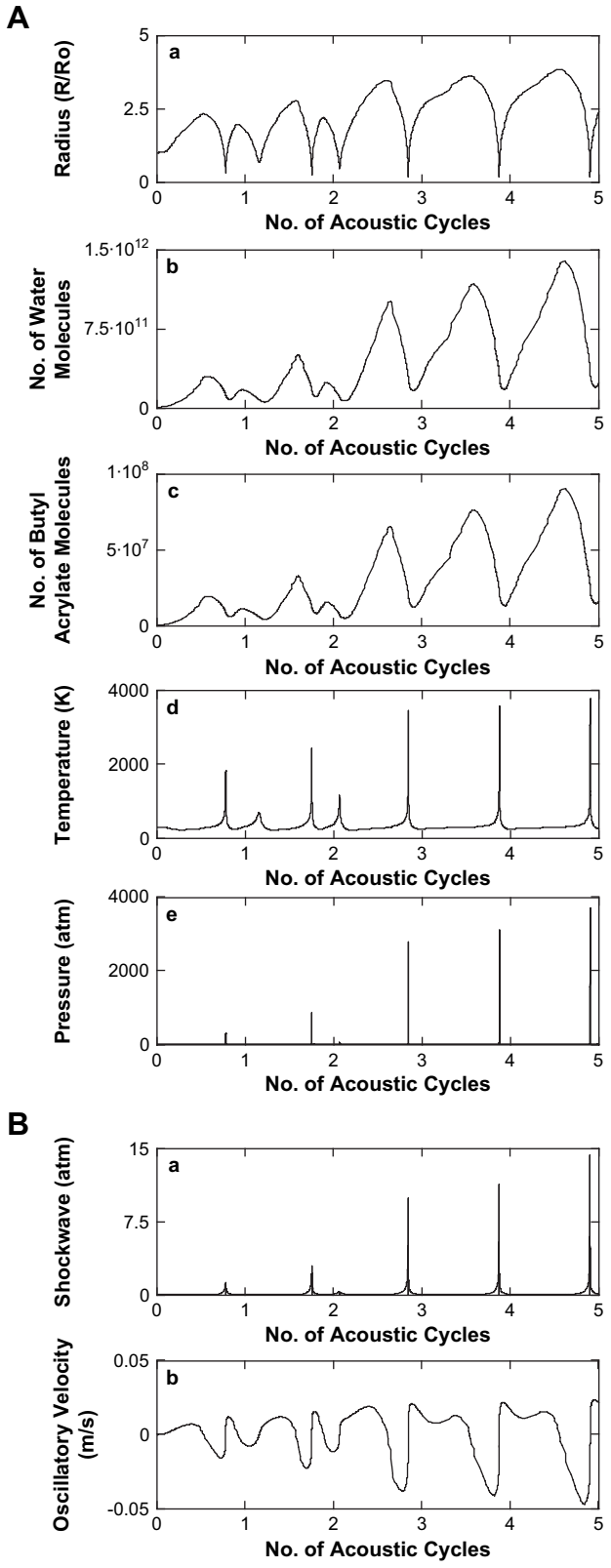

Fig. 5. (A) Simulation of the radial motion of a 20 μm nitrogen bubble in a solution of butyl acrylate monomer. Time variation of (a) normalized bubble radius (R/R_0); (b) number of water molecules in the bubble; (c) number of butyl acrylate molecules in the bubble; (d) temperature in the bubble; (e) pressure in the bubble. (B) Simulation of the physical effect induced by the bubble. Time variation of (a) shock wave emitted by the bubble and (b) oscillatory velocity or microturbulence.

wider spectrum of species, which include monomeric free radicals such as $CH_3^{\bullet}$ in addition to the $H^{\bullet}$ and $OH^{\bullet}$ radicals formed out of dissociation of water molecules trapped in the bubble.

6. Discussion

Correlating the experimental and simulations results helps reveal some interesting features of the sonochemical emulsion polymerization of butyl acrylate and vinyl acetate. However, prior to making such correlation, we would like to ponder over physical parameters that influence the particle size distribution in the emulsion polymerization reaction system and the relative magnitudes of this influence anticipated for the different combinations of experimental conditions.

Ultrasonic shear velocity or microturbulence: The ultrasonic shear velocity or the velocity of microturbulence generated by the cavitation bubble influences the dispersion of monomer into droplets. The larger the microturbulence velocity, the larger the shear force responsible for dispersion of monomer and the finer the droplet. As sonication begins, initially the monomer droplets are expected to have a wide size distribution. However, as shearing action continues, this size distribution narrows down – provided the conversion of monomer to polymer occurs at a slower rate. Moreover, the process of shearing is fast and continuous. Under these circumstances, the unreacted monomer is continuously convected and dispersed in the medium giving further nucleation, without forming feed to the polymer particles formed out of polymerization, which would make these particles grow. Collision between and coalescence of the droplets may as well act towards widening of the size distribution of droplets, but shearing action of ultrasound can easily reverse it. As the simulation results reveal, microturbulence velocity and shearing action are higher for the saturated medium than that for unsaturated medium.

Concentration of radicals: The rate of polymerization depends on the concentration of radicals in the medium. At high concentration of radicals (for a moderately reactive polymer) the monomer droplets are *spot* polymerized. Thus, the sizes of the droplet and the polymer particle essentially match. In such a situation, a wider size distribution of droplets results in wider size distribution of particles. On the contrary, if the concentration of radicals is low, the rate of polymerization is also low. In such situations, the monomer droplet may not be completely spot polymerized. The unreacted monomer from the droplet may diffuse away or may be convected away from the droplet with the continuous shearing action resulting in nucleation of newer droplets. A small average but uniform particle size is expected for these conditions. From simulation results, one can perceive that concentration of radicals will be much higher for an unsaturated medium than that for the saturated one.

Glass transition temperature: This factor influences the coalescence of polymer particles. If the polymer has a low glass transition temperature, the particle is soft and rubbery which lead to coalescence between particles following collision. On the contrary, if the particle has high glass transition temperature, it would be glassy – not favoring coalescence.

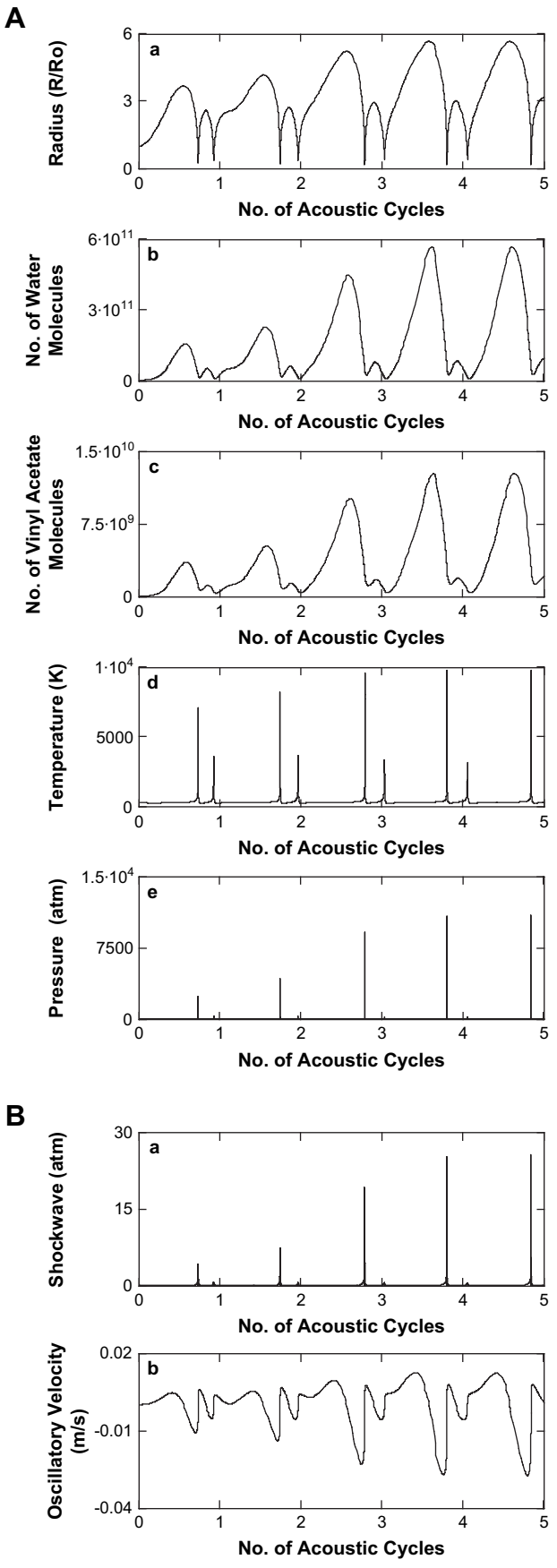

The glass transition temperature for butyl acrylate is −54 °C while that of vinyl acetate is 32 °C. Therefore, at the experimental conditions (with temperature variation in range 30 ± 5 °C), polymer particles of both VA and BA are expected to be in the rubbery state – favoring coalescence. However, on a relative basis, the tendency of coalescence will be far higher for PBA.

Shock waves: The shock waves generated by the bubble act towards the disruption and scattering of polymer particles. The higher the magnitude of the shock wave, the higher the disruption of the polymer particles into fragments with wide size range, which gets scattered in the bulk. During scattering, these may collide and coalesce. Thus, the shock waves basically widen the size distribution of the particles. However, whether shock waves can disintegrate the polymer particle depends on the relative dimensions (or scale) of the particle and shock wave. A typical cavitation bubble of radius ~10 μm is compressed to 1/10th of its original size at the instance of maximum compression. The shock wave emerging from it is also of similar dimensions. If the polymer particle is too small (~100 nm) it is not likely to be disrupted by the shock wave – as the dimension of the shock wave is far too large. Instead, it will be drifted away with the shock wave. On the other hand, polymer particles of size >10 μm are likely to be disintegrated by the force exerted by the shock wave. Simulation results indicate that the magnitude of the shock waves is much higher in an unsaturated medium. Moreover, argon bubbles are seen to generate more intense shock waves.

Population density of particles in the medium: For large population density of polymer particles, the probability of particle–particle collision is high that leads to coalescence between them. If the particles grow to micrometer size after coalescence, they will be disrupted by the shock waves, as a result of which the particle size distribution widens. For relatively low concentration of radicals, the rate of polymerization is small and large population density of particles would be seen only for longer duration of sonication. However, if the radical concentration is high, the polymerization rate would be rapid – resulting in spot polymerization of monomer droplets. Accordingly, large population density of particles can be seen for relatively short sonication periods. On this basis, one can expect large population density of particles in an unsaturated medium, with high concentration of radicals, which ultimately results in wide particle size distribution.

It can be perceived that some of these factors have opposite effects on the particle size distribution. For example, ultrasonic shear velocity or microturbulence tries to narrow down the polymer particle size distribution, while the shock waves try to widen it. Therefore, the polymer particle size resulting for a particular combination of experimental conditions is a result

Fig. 6. (A) Simulation of the radial motion of a 10 μm argon bubble in a solution of vinyl acetate monomer. Time variation of (a) normalized bubble radius (R/R_0); (b) number of water molecules in the bubble; (c) number of vinyl acetate molecules in the bubble; (d) temperature in the bubble; (e) pressure in the bubble. (B) Simulation of the physical effect induced by the bubble. Time variation of (a) shock wave emitted by the bubble and (b) oscillatory velocity or microturbulence.

Table 2
Simulation results for butyl acrylate solution

	Parameters for simulation			
	$R_0 = 10$ μm argon bubble	$R_0 = 20$ μm argon bubble	$R_0 = 10$ μm nitrogen bubble	$R_0 = 20$ μm nitrogen bubble
	Conditions at the first compression of the bubble			
	$T_{max} = 7690$ K	$T_{max} = 2823$ K	$T_{max} = 3841$ K	$T_{max} = 1835$ K
	$P_{max} = 3497$ atm	$P_{max} = 156.4$ atm	$P_{max} = 4355$ atm	$P_{max} = 321.2$ atm
	$N_{WT} = 2.84E + 010$	$N_{WT} = 1.279E + 011$	$N_{WT} = 2.48E + 010$	$N_{WT} = 1.223E + 11$
	$N_{MT} = 2.35E + 06$	$N_{MT} = 9.641E + 06$	$N_{MT} = 1.83E + 06$	$N_{MT} = 8.783E + 06$
	Physical effect produced by the bubble			
	$V_{turb} = 0.0195$ m/s	$V_{turb} = 0.032$ m/s	$V_{turb} = 0.012$ m/s	$V_{turb} = 0.035$ m/s
	$P_{shock} = 24.9$ atm	$P_{shock} = 6.14$ atm	$P_{shock} = 19.52$ atm	$P_{shock} = 14.26$ atm
	Equilibrium composition of different species in the bubble at collapse (mole fraction)			
H_2	4.4619E-01	2.1834E-02	5.7501E-01	1.3304E-03
CO	3.3542E-01	6.9855E-05	3.7036E-01	2.5836E-06
H	1.8337E-01	1.0421E-03	1.3656E-02	0
H_2O	1.1354E-02	9.5581E-01	2.8061E-02	9.9811E-01
OH	4.8980E-03	1.3381E-02	3.7517E-04	5.3004E-05
HCO	3.5818E-03	0	8.6903E-04	0
C_2H_2	3.5279E-03	0	2.6442E-03	0
C_2H	2.7099E-03	0	1.1384E-04	0
CH_2	1.8309E-03	0	1.0560E-04	0
CH_3	1.7959E-03	0	1.9060E-03	0
CH	1.3667E-03	0	5.1623E-06	0
O	1.0702E-03	3.9401E-04	5.0211E-06	0
CO_2	9.3458E-04	4.4763E-04	2.1619E-03	4.9824E-04
C	8.0900E-04	0	0	0
C_2O	3.4689E-04	0	1.0155E-05	0
H_2CO	3.0475E-04	0	5.2226E-04	0
CH_4	2.6226E-04	0	3.9204E-03	0
C_2	1.1062E-04	0	0	0
C_2H_3	7.0303E-05	0	6.1999E-05	0
C_2H_4	2.1507E-05	0	2.0478E-04	0
C_3	1.1218E-05	0	0	0
O_2	1.0387E-05	6.9683E-03	0	9.4993E-06
C_3O_2	2.5502E-06	0	1.4805E-06	0
HOO	1.2380E-06	4.0405E-05	0	0
CH_2CO	0	0	1.7647E-06	0
CH_3OH	0	0	1.6725E-06	0
H_2O_2	0	1.2483E-05	0	0
	Total amount of H, OH and CH_3 radicals produced per bubble			
	5.398E + 09	1.845E + 09	3.953E + 08	6.483E + 06

of simultaneous and competing actions of various factors mentioned. Based on the above contemplations, we now try to explain the trends seen in particle size distribution for various combinations of experimental parameters.

6.1. Experiments with saturated medium

As indicated by the simulation results, for a saturated medium, the rate of radical production is relatively smaller than that of unsaturated medium (we would like to mention that this conclusion has been supported by results of our earlier study using Weissler reaction as a model, Sivasankar et al. [23]). However, the microturbulence or shear velocity is high; approximately twice that of the unsaturated medium. As a result of these conditions, the polymerization rate is low and the monomer is dispersed in the medium in the form of fine droplets, which are spot polymerized by the radicals. The population density of polymer particles during sonication period does not rise appreciably resulting in lesser collision–coalescence–disruption of polymer particles, which would widen the particle size distribution. The final outcome is a smaller polymer particle size, which stays more or less constant during 20 min of sonication. Comparing among nitrogen and argon as bubbling gas, one would expect higher polymerization rate with argon bubbling as the radical production rate from argon bubbles is three orders of magnitude higher than that from nitrogen bubbles. This results in faster spot polymerization of relatively larger monomer droplets before they are dispersed in the medium into finer droplets as sonication proceeds. Comparing between the two monomers, PBA particles are seen to have somewhat larger size than PVA particles. We attribute this result to the moderate level of coalescence between particles. Although the probability of collision among polymer particles is similar for PBA and PVA particles, due to lower glass transition temperature, the tendency to coalesce will be greater for PBA particles resulting in slightly larger size.

Table 3
Simulation results for vinyl acetate solution

	Parameters for simulation			
	$R_0 = 10$ μm argon bubble	$R_0 = 20$ μm argon bubble	$R_0 = 10$ μm nitrogen bubble	$R_0 = 20$ μm nitrogen bubble
	Conditions at the first compression of the bubble			
	$T_{max} = 7072$ K	$T_{max} = 2337$ K	$T_{max} = 4084$ K	$T_{max} = 1704$ K
	$P_{max} = 2424$ atm	$P_{max} = 89.5$ atm	$P_{max} = 4963$ atm	$P_{max} = 245.7$ atm
	$N_{WT} = 2.49E+010$	$N_{WT} = 1.16E+011$	$N_{WT} = 2.7E+010$	$N_{WT} = 1.12E+011$
	$N_{MT} = 1.087E+09$	$N_{MT} = 3.481E+09$	$N_{MT} = 1.086E+09$	$N_{MT} = 3.314E+09$
	Physical effect produced by the bubble			
	$V_{turb} = 0.0195$ m/s	$V_{turb} = 0.023$ m/s	$V_{turb} = 0.012$ m/s	$V_{turb} = 0.021$ m/s
	$P_{shock} = 25.52$ atm	$P_{shock} = 2.443$ atm	$P_{shock} = 19.43$ atm	$P_{shock} = 3.88$ atm
	Equilibrium composition of different species in the bubble at collapse (mole fraction)			
H_2	3.8177E-01	1.6709E-01	5.1610E-01	1.7659E-01
CO	3.7713E-01	5.5469E-02	4.2637E-01	4.4314E-02
H	2.0372E-01	5.0243E-04	1.8653E-02	4.0788E-06
H_2O	1.6381E-02	7.3308E-01	2.1217E-02	7.2521E-01
OH	9.1753E-03	3.8106E-04	4.7938E-04	0
HCO	3.1014E-03	0	1.3504E-03	0
C_2H_2	6.4493E-04	0	5.5317E-03	0
C_2H	6.4327E-04	0	3.6680E-04	0
CH_2	7.2412E-04	0	2.3371E-04	0
CH_3	5.4699E-04	0	2.7323E-03	0
CH	7.0185E-04	0	1.6961E-05	0
O	2.6032E-03	0	9.6335E-06	0
CO_2	1.7717E-03	4.3471E-02	2.0445E-03	5.3872E-02
C	5.3947E-04	0	2.4116E-06	0
C_2O	1.8028E-04	0	3.1056E-05	0
H_2CO	2.0322E-04	0	6.1520E-04	1.4366E-06
CH_4	0	0	3.7936E-03	9.9876E-06
C_2	3.4096E-05	0	0	0
C_2H_3	9.8977E-06	0	1.3688E-04	0
C_2H_4	2.3318E-06	0	3.1211E-04	0
C_3	1.5982E-06	0	0	0
O_2	4.2601E-05	1.3949E-06	0	0
C_3O_2	1.0329E-06	0	3.7715E-06	0
HOO	3.9102E-06	0	0	0
CH_2CO	0	0	2.1447E-06	0
CH_3OH	0	0	1.4993E-06	0
H_2O_2	0	0	0	0
	Total amount of H, OH and CH_3 radicals produced per bubble			
	5.546E + 09	1.056E + 08	6.141E + 08	4.7E + 05

Note: The number format is as follows: 4.4619E-01 should be read as 4.4619×10^{-1}. Species having equilibrium mole fraction less than 10^{-6} have been ignored. An equilibrium bubble size (R_0) of 10 μm represents unsaturated medium while an equilibrium bubble size of 20 μm represents saturated medium. Various notations used are as follows: T_{max} − temperature peak reached in the bubble at the time of first collapse; P_{max} − pressure peak reached in the bubble at the time of first collapse; N_{WT} − number of water molecules trapped in the bubble at the instance of first collapse; N_{MT} − number of monomer molecules trapped in the bubble at the instance of first collapse; V_{turb} − velocity of the microturbulence generated by the bubble (calculated as the mean of positive, i.e. away from bubble; and negative i.e. towards bubble, velocity); P_{shock} − pressure amplitude of the shock wave generated by the bubble.

6.2. Experiments with unsaturated medium

For the unsaturated medium, the rate of radical production is very high (one to three orders of magnitude higher than saturated medium), while the microturbulence or shear velocity is small. These two conditions lead to some interesting effect on the sonochemical polymerization system. Due to smaller shear velocity the monomer is dispersed into relatively larger droplets. However, large concentration of radicals gives rapid polymerization of these droplets resulting in polymer particle of larger size. Moreover, the population density of polymer particles in the medium also rises quickly due to faster polymerization. Consequently, the probability of collision and coalescence between particles rises. As the polymer particle size reaches micrometer range, the phenomenon of disruption due to shock waves is onset. Thus, the particle size distribution in the system at any instance increases and the mean particle size fluctuates significantly with time. Despite this, the mean particle size for both PBA and PVA is larger than the corresponding size in a saturated medium. This is indicative of the fact that over 20 min of sonication, the phenomenon of collision−coalescence between polymer particles leading to growth of the particles overwhelms the disruptive action of shock waves, which reduces the mean particle size. Comparing among nitrogen and argon as bubbling gas, much larger fluctuation in mean particle size and particle size distribution

is seen for argon than for nitrogen. This is clearly attributed to higher radical production and generation of higher intensity shock waves by the argon bubbles, which result in faster polymerization (giving larger population density of polymer particles in the medium) and higher coalescence–disruption of polymer particles. Comparing between monomers, we see larger oscillations of mean particle size and particle size distribution for PBA particles than for PVA particles. We ascribe this to greater tendency of coalescence (followed by shock wave induced disruption) between PBA particles than PVA particles. Although the mean size of the PBA particles for nitrogen bubbling is larger than PVA particles all along 20 min of sonication, an interesting leveling-off between the mean sizes of PBA and PVA particle is seen for argon bubbling after 20 min of sonication. We explain this result in terms of differences between intensities of the shock waves generated by argon and nitrogen bubbles. As noted earlier, the extent of coalescence induced growth is different for PBA and PVA particles – with greater coalescence for PBA particles (due to lower glass transition temperature) resulting in larger particle size than PVA. Although the degree of coalescence between PBA particles is expected to be similar for both bubbling gases, more intense shock waves induced by argon bubbles cause greater disruption of the PBA particles (than the relatively milder shock waves induced by nitrogen bubbles). Thus, the mean particle sizes of PBA and PVA get leveled off for 20 min of sonication, although particle size distribution is broader for PBA particles (indicated by a wider error bar) than for PVA particles.

7. Conclusion

This article provides a physical insight into the sonochemical emulsion polymerization by bridging the physics and chemistry of the system. Our analysis is mainly focused on the mean size and size distribution of the polymer particles resulting out of polymerization reaction – as this is the essential and ultimate manifestation of the sonochemical phenomenon in the reaction system. Experiments with combinations of various conditions (type of monomer, bubbling gas and saturation level of the medium) coupled to a bubble dynamic model that takes into account the heat and mass transfer reveal interesting physical features of the sonochemical polymerization system. The mean size and size distribution of the polymer particles are found to be a complex function of various physical and chemical parameters such as extent of radical production from cavitation bubbles, magnitude of microturbulence or shear velocity and shock waves produced by the bubbles, glass transition temperature of the polymer and the population density of the polymer particles. These parameters show significant variation with different experimental conditions, and some of them have reverse effects on the polymerization system. The final outcome of the polymerization reaction is found to be a manifestation of simultaneous and competing influence of these parameters. This article gives a semi-quantitative account of this influence with a combined experimental-modeling approach, which can be extended to any other emulsion polymerization system.

Acknowledgments

Authors gratefully acknowledge valuable suggestions in the bubble dynamic modeling and analysis from Professor Franz Grieser and Dr. M. Ashokkumar (Particle Fluids Processing Center, School of Chemistry, University of Melbourne, Australia) and Professor Andrea Prosperetti (Department of Mechanical Engineering, Johns Hopkins University, USA). Authors also thank Center for Nanotechnology, I.I.T. Guwahati and Center for Material Characterization, National Chemical Laboratory, Pune for providing analytical facilities.

References

[1] Kruus P, Patraboy TJ. Journal of Physical Chemistry 1985;89:3379–84.
[2] Kruus P, McDonald D, Patraboy TJ. Journal of Physical Chemistry 1987;89:3041–7.
[3] Price GJ, Norris DJ, West PJ. Macromolecules 1992;25:6447–54.
[4] Biggs G, Grieser F. Macromolecules 1995;28:4877–82.
[5] Cooper G, Grieser F, Biggs G. Journal of Colloid and Interface Science 1996;184:52–63.
[6] Ooi SK, Biggs S. Ultrasonics Sonochemistry 2000;7:125–33.
[7] Bradley M, Grieser F. Journal of Colloid and Interface Science 2002;251:78–84.
[8] Xia HS, Wang Q, Liao YQ, Xu X, Baxter SM, Slone RV, et al. Ultrasonics Sonochemistry 2002;9:151–8.
[9] Price GJ, Lenz EJ, Ansell CWG. European Polymer Journal 2002;38:1531–6.
[10] Zhang C, Wang Q, Xia H, Qiu G. European Polymer Journal 2002;39:1769–76.
[11] Zhang C, Cao Y, He Y. Journal of Applied Polymer Science 2004;94:763–8.
[12] Yin N, Chen K, Kang W. Ultrasonics Sonochemistry 2006;13:345–51.
[13] Teo BM, Prescott SW, Ashokkumar M, Grieser F. Ultrasonics Sonochemistry 2007; doi:10.1016/j.ultsonch.2007.01.009.
[14] Lindstrom O, Lamm O. Journal of Physical and Colloid Chemistry 1951;55:1139–46.
[15] Henglein A, Schulz R. Zeitschrift fur Naturforschung 1952;7B:484–5.
[16] Henglein A. Makromolekulare Chemie 1954;14:15–39.
[17] Suslick KS, editor. Ultrasound: its chemical, physical and biological effects. New York: VCH Publishers; 1988.
[18] Mason TJ, Lorimer JP. Sonochemistry: theory, application and uses of ultrasound in chemistry. New York: Ellis Horwood; 1989.
[19] Shah YT, Pandit AB, Moholkar VS. Cavitation reaction engineering. New York: Plenum Press; 1999.
[20] Hart EJ, Henglein A. Journal of Physical Chemistry 1985;89:4342–7.
[21] Hart EJ, Henglein A. Journal of Physical Chemistry 1987;91:3654–6.
[22] Suslick KS. Science 1990;247:1439–45.
[23] Sivasankar T, Paunikar AW, Moholkar VS. AIChE Journal 2007;53:1132–43.
[24] Kamath V, Prosperetti A, Egolfopoulos FN. Journal of Acoustical Society of America 1993;94:248–60.
[25] Prasad Naidu DV, Rajan R, Kumar R, Gandhi KS, Arakeri VH, Chandrasekaran S. Chemical Engineering Science 1994;49:877–88.
[26] Rajan R, Kumar R, Gandhi KS. Chemical Engineering Science 1998;53:255–71.
[27] Sochard S, Wilhelm AM, Delmas H. Ultrasonics Sonochemistry 1997;4:77–84.
[28] Yasui K. Physical Review E 1997;56:6750–60.
[29] Yasui K. Journal of Physical Society of Japan 1997;66:2911–20.
[30] Gong C, Hart DP. Journal of Acoustical Society of America 1998;104:2675–82.
[31] Moss WC, Yound DA, Harte JA, Levalin JL, Rozsnyai BF, Zimmerman GB, et al. Physical Review E 1999;59:2986–92.

[32] Storey BD, Szeri AJ. Proceedings of the Royal Society of London Series A 2000;456:1685–709.
[33] Toegel R, Gompf B, Pecha R, Lohse D. Physical Review Letters 2000;85:3165–8.
[34] Ilyichev VI, Koretz VL, Melnokov NP. Ultrasonics 1989;27:357–61.
[35] Storey BD, Szeri AJ. Proceedings of the Royal Society of London Series A 2001;457:1685–700.
[36] Brennen CE. Cavitation and bubble dynamics. Oxford: Oxford University Press; 1995.
[37] Prosperetti A, Lezzi A. Journal of Fluid Mechanics 1986;168:457–77.
[38] Hsieh DY, Plesset MS. Journal of Acoustical Society of America 1961;33:206–15.
[39] Eller AI, Flynn HG. Journal of Acoustical Society of America 1965;37:493–503.
[40] Safar MH. Journal of Acoustical Society of America 1968;43:1188–9.
[41] Lofstedt R, Weninger K, Puttermann SJ, Barber BP. Physical Review E 1995;51:4400–10.
[42] Fyrillas M, Szeri AJ. Journal of Fluid Mechanics 1994;277:381–407.
[43] Crum LA. Journal of Acoustical Society of America 1980;68:203–11.
[44] Fyrillas M, Szeri AJ. Journal of Fluid Mechanics 1995;289:295–314.
[45] Lee J, Kentish S, Ashokkumar M. Journal of Physical Chemistry B 2005;109:14595–8.
[46] Bapat PS, Gogate PR, Pandit AB. Ultrasonics Sonochemistry 2007; doi:10.1016/j.ultsonch.2007.08.002.
[47] Kumar KS, Moholkar VS. Chemical Engineering Science 2007;62: 2698–711.
[48] Krishnan SJ, Dwivedi P, Moholkar VS. Industrial and Engineering Chemistry Research 2006;45:1493–504.
[49] Hirschfelder JO, Curtiss CF, Bird RB. Molecular theory of gases and liquids. New York: Wiley; 1954.
[50] Wilke CR. Journal of Chemical Physics 1950;18:517–9.
[51] Condon EU, Odishaw H. Handbook of physics. New York: McGraw Hill; 1958.
[52] Leighton TG. The acoustic bubble. San Diego: Academic Press; 1994.
[53] Young FR. Cavitation. London: McGraw Hill; 1989.
[54] Press WH, Teukolsky SA, Flannery BP, Vetterling WT. Numerical recipes. New York: Cambridge University Press; 1992.
[55] Prosperetti A, Commander KW. Journal of Acoustical Society of America 1989;85:732–46.
[56] Eriksson G. Chemica Scripta 1975;8:100–3.